A phenomenological interpretation of multiple bursting patterns in Lateral Habenula neurons

Dmitry Fedorov[1], Fabien Campillo[2], Mathieu Desroches[2,3], Edgar Soria-Gómez[1], Joaquin Piriz[1,4,*], and Serafim Rodrigues[3,4,*]

[1]Achucarro Basque Center for Neuroscience, Leioa, Basque Country, Spain
[2]MathNeuro, Inria Branch of the University of Montpellier, Montpellier, France
[3]MCEN, BCAM - Basque Center for Applied Mathematics, Bilbao, Spain
[4]Ikerbasque - The Basque Foundation for Science, Bilbao, Spain
[*]Joaquin.Piriz@achucarro.org, srodrigues@bcamath.org

January 23, 2025

Abstract

We present lateral habenula (LHb) neural data that display a variety of bursting patterns, with two dominant types and a third one that appears as a mix of the other two. We analyse these patterns using elementary statistical tools and characterise them from the perspective of average frequency during the burst and burst duration, which yields two main categories. We then propose an idealised multiple-timescale dynamical model that captures the two main types of bursting patterns observed in the data, namely *square-wave* and *parabolic* bursting, as well as the intermediate *mixed-type* (also termed *triangular*) bursting. We identify a special point in parameter space, termed *saddle-node homoclinic*, which acts as an organising center to distinguish between the two main bursting patterns. Finally, we relate the bursting categories inherent to the model and those identified through statistical analysis, discussing their possible convergence and limitations.

Keywords: Lateral Habenula neurons; patch-clamp electrophysiology; excitability; bursting patterns; multiple-timescale dynamics; bifurcation theory.

1 Introduction

The Lateral Habenula (LHb) is a highly conserved structure in the vertebrate brain, located within the epithalamus. It serves as a crucial communication hub between the limbic system and the midbrain, integrating inputs from various limbic structures. The LHb exerts a potent inhibitory influence on serotonergic and dopaminergic systems through both direct and indirect pathways. Notably, it exhibits robust responses to a wide range of aversive or potentially noxious stimuli, earning its designation as an "anti-reward" encoding center.

Hyperactivity of the LHb has been implicated in several psychiatric disorders characterized by heightened aversion, particularly depression [13]. Indeed, the LHb has been proposed as a key brain target underlying the antidepressant effects of ketamine [4]. Additionally, its direct modulation through deep-brain stimulation is currently being explored as a potential treatment for depression [1].

The LHb is predominantly composed of small glutamatergic neurons with high input resistance ($> 500\text{M}\Omega$) that receive both glutamatergic and GABAergic inputs. In vitro, these neurons exhibit complex patterns of spontaneous spiking activity, which have been qualitatively categorized into four modes: silent, non-regular tonic spiking, regular tonic spiking and bursting [29]. However, LHb neurons can transition between these patterns, suggesting that these modes are not associated with different neuronal classes but with specific dynamic states.

Among these activity modes, silent and tonic patterns are the most prominent, while only a minority of neurons ($< 10\%$) display spontaneous bursting activity. However, the majority ($\sim 90\%$) of LHb neurons exhibit rebound bursting after negative current injection, indicating that bursting is a general property, although largely latent, of LHb neurons. Bursting activity at the LHb has drawn significant attention because of its association with depression-like states in animal models.

In such models, the proportion of LHb neurons that exhibit bursting activity increases. Moreover, inducing bursting activity replicates depressive-like behaviors, whereas drugs that block bursting, most notably ketamine, have been shown to counteract these effects [3, 4, 6, 7, 14, 19, 22, 26, 30].

However, the specific reasons why LHb bursting activity is linked to depression-like states remain unclear. Bursting activity is characterized by a temporal alternation between periods of high-frequency firing and quiescence. This implies a temporal arrangement of the neuronal output, but not necessarily an increase in overall neuronal output. Thus, from a functional perspective, it is not immediately apparent why the bursting activity of the LHb contributes to depressive states. Moreover, LHb bursting activity has been primarily described in broad terms as periods of heightened firing [4, 7, 20, 30], lacking the detailed analyses and classifications that have been developed for bursting activity in other neural contexts [9, 15]. Thus, as currently defined, LHb bursting activity may encompass diverse activity states, each potentially linked to depressive states in different ways. These gaps in understanding highlight the need for modeling approaches that capture the diversity of LHb activity patterns. Here, we address this by presenting an initial phenomenological model to describe the activity of LHb neurons.

From a neurodynamics perspective, we observed a gradient of bursting patterns ranging from *square-wave* to *parabolic* bursts, as well as intermediate forms referred to as *triangular*; see below for details. Notably, previous criteria used to define bursting activity in the LHb have primarily encompassed square-wave bursts, potentially overlooking parabolic and intermediate patterns seemingly characterized by lower frequencies and longer durations and different shaped captured by the computational model. Furthermore, we recorded neurons in which these three bursting patterns spontaneously emerged over time, along with tonic and irregular spiking activity, suggesting that these patterns may represent dynamic states of the same neurons.

To account for this diversity of dynamical behaviors, we propose a minimal phenomenological model capable of capturing these patterns. The model incorporates an organizing center in parameter space, enabling transitions between different behaviors driven by two main slow processes at play in the system. We further conjecture that these bursting patterns arise from distinct sets of conductances, representing different modes of information transmission by LHb neurons, each with potentially unique implications for aversion encoding.

2 Materials and methods

2.1 Animals

Experiments were performed in adult (6-9 months) male C57BL/6JRj mice of from Janvier Labs (France). Animals were kept at the animal facility of the University of the Basque Country, Bizkaia Campus under controlled temperature and humidity conditions with a 12/12 hours dark-light cycle. Food and drinking water were available ad libitum. All procedures followed the European Directive 2010/63/EU, NIH guidelines and were approved by the Ethics Committees of the University of the Basque Country EHU/UPV (Leioa, Spain; CEEA M20/2024/213).

2.2 Electrophysiology

2.2.1 Preparation of brain slices

Mice were anesthetized with isoflurane (IsoFlo 100%, Zoetis), and quickly decapitated into chilled and gassed NDMG-prep solution [27]. The brain was extracted and sliced on a vibratome (VT1000S or VT1200S, Leica) in the same solution to a thickness of 250 µm. The slices were then recovered in 36°C NMDG-prep solution for 40 minutes, with gradual introduction of Na^+ into solution following the Na^+ spike-in procedures described by [27]. The slices were then transferred to room temperature HEPES-based storage solution for the day.

2.2.2 Patch-clamp recordings

Patch-clamp experiments were carried out with CleverExplore Neuroscience Workstation (MCI Neuroscience), including 10x air (CP-Achromatic, Zeiss) and 40x water-immersion (LUMPlanFL, Nikon) objectives, DIC optics, digital camera (MCI-CXE-B013-U), and EPC-10 USB Double amplifier (HEKA Electronics) using PatchMaster v. 2x92. The recording solution contained (in mM): 2.5 KCl, 1.25 NaH_2PO_4, 25 $NaHCO_3$, 17 glucose, 125 NaCl, 2 $CaCl_2$, and 1 $MgCl_2$, feeding at a rate of 2.5 ml/min. The recordings were made at the average temperature of 29.5 ± 1.5°C. The internal solution of glass pipettes (GB150F-10, Science Products, 5.5–9 MΩ) contained (in mM):

130 K-gluconate, 5 KCl, 10 HEPES, 0.6 EGTA, 2.5 $MgCl_2$, 10 phosphocreatine, 4 ATP-Mg, and 0.4 GTP-Na_3.

Electrophysiological data was collected using Patchmaster software (HEKA Electronics) in whole-cell mode. After membrane breaking-in, cells were left to stabilize without current injection for 3 minutes. After this period, the spontaneous activity was recorded for at least 1 minute in the current-clamp configuration. Following that, additional current clamp recordings were carried out during which the neuron responses to injected current was evaluated. The current was injected in 11 steps, with the initial step bringing the cell to approximately −80 mV and the final step to approximately −40 mV. Cells with membrane potential under −40 mV were excluded from analysis. The collected data was converted to .abf format and analyzed using Igor Pro v. 9.0.5.1, pClamp 10.7 (Molecular Devices), Matlab (MathWorks) as well as the Python module pyABF [1].

2.3 Analysis

2.3.1 Spike detection

Spike detection was carried out using the Igor Pro software with the Neuromatic toolkit [25] using threshold detection at half-peak height.

2.3.2 Burst detection

Recent work has defined LHb bursting activity based on the absolute instantaneous frequency [7, 30, 4], setting up a cell independent threshold for initiating and terminating the burst. This definition does account for bursting activity being defined as an increase in the spiking frequency that deviates from the basal. Therefore, we applied a statistical criterion consisting in a simplified version of the *Poisson Surprise Method* [18] that defines bursts as unexpectedly short inter-spike intervals.

Assuming a Poisson distribution we calculated cumulative probability of observing one event for each inter-spike interval using the following formula:

$$P = \mathrm{e}^{-\lambda}(1 + \lambda),$$

where λ is the product of the mean firing rate by the inter-spike interval.

Hence the Surprise index S was calculated as:

$$S = -\log P.$$

To mark the beginning of the burst, we set up a threshold of $P \leq 0.005$ ($S = 2.3$). Since bursts are defined by an abrupt increase in spiking frequency that attenuates, we set up a lower threshold to define the end of a burst at twice the basal frequency ($S = 1.045$).

2.3.3 Statistics

Statistical analysis was carried out using RStudio v.2023.12.0 Build 369. *Shapiro-Wilk* test was used to determine data normality, *Levene*'s test was used to determine homogeneity of variance. For comparisons, in case of normally distributed samples with equal variance a two samples unpaired t-test was used. In case one or more of variables being non-normally distributed a two samples *Wilcoxon* test was used.

2.4 Computational model

In the modeling part of this work, we choose to focus on one particular aspect of the recorded data, namely the presence of two main types of bursting patterns together with a third one that is intermediate between the other two. The right panels of Fig. 1 show the outputs of the model corresponding to each of these three bursting patterns, namely square-wave (top), parabolic (center) and mixed-type or triangular (bottom); the left panels show recordings displaying the three different bursting behaviors. To identify these different bursting patterns in the computational model, we follow the standard approach introduced by J. Rinzel [24], termed *slow-fast dissection*, and apply it to an extended version of a classical three-dimensional phenomenological bursting model called the Hindmarsh-Rose (HR) model [12]. The initial model from [12] has two fast variables,

[1] https://github.com/swharden/pyABF

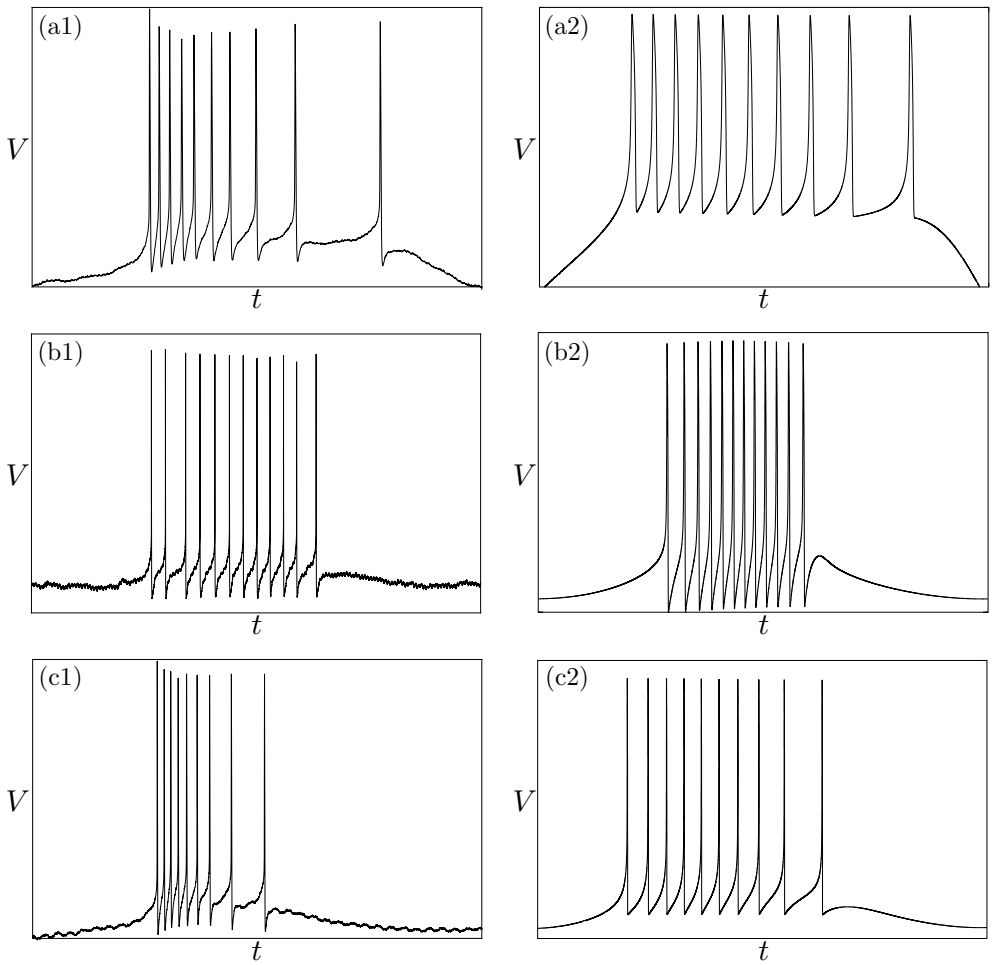

Figure 1: Experimental data (left panels) vs. mathematical model (1) (right panels), showing three bursting patterns identified in LHb neurons and captured by our idealised model. Namely: (a1)-(a2) square-wave bursting; (b1)-(b2) parabolic bursting; (c1)-(c2) triangular (mixed) bursting, at the transition between the other two patterns (see also Fig. 4). Fixed parameter values are: $a = 0.08$, $c = 3$, $d = 1.8$, $\varepsilon = 0.01$, $s = 0.01$, $x_1 = -3$. Case-specific parameter values are: (a2) $b_0 = 0.52$, $z_0 = -0.7163$, $\alpha = -0.1$; (b2) $b_0 = 1.5$, $z_0 = -1.75$, $\alpha = -0.1$; (c2) $b_0 = 0.75$, $z_0 = -2$, $\alpha = 0.003$.

which can be associated with membrane potential and fast ionic dynamics, as well as one slow variable associated with slow ionic dynamics. We extend the model by adding a second slow variable, which can be related to an additional slow current, in order to capture parabolic bursting [8, 24].

In the case of models with two slow variables, the slow-fast dissection method consists in relating the bursting pattern produced by the complete model, projected onto a plane formed by the slow variables, with the two-parameter bifurcation diagram of the so-called *fast subsystem* obtained when freezing the dynamics of the slow variable and considering them as parameters in the fast differential equations. That particular bifurcation structure is the signature of the corresponding patterns, it allows to characterize it and, hence, to classify bursting patterns [9, 15, 24]. More precisely, one only needs two bifurcations of the fast subsystem in order to fully characterize a given bursting patterns, namely one bifurcation that organizes the transition between quiescence and burst in the complete model, and another bifurcation organizing the reverse transition.

According to the classification system introduced by Rinzel, square-wave bursting is associated with a saddle-node bifurcation of equilibria, initiating the burst, and a saddle homoclinic bifurcation terminating it. Note that this bursting pattern requires only one slow variable but it can also be obtained in a model with two slow variables. In contrast, parabolic bursting requires minimally two slow variables, and it corresponds to a bursting case in which both the initiation and termination of the burst in the full system are caused by the same bifurcation in the fast subsystem, namely, a saddle-node on invariant circle (SNIC) bifurcation. To be more precise, parabolic bursting is associated with a family of SNIC bifurcations in the fast subsystem, depending on two parameters. Hence, the full system has minimally two fast and two slow variables, unlike minimal

square-wave bursting models, which have only one slow variable. Therefore, for the original three-dimensional HR model (with one slow variable) to sustain parabolic-bursting activity, we need to augment it by one differential equation, which will correspond to an additional slow ionic variable. As mentioned above, such a four-dimensional model can also sustain square-wave bursting patterns, single saddle-node and homoclinic bifurcations of the fast subsystem being replaced by curves of such bifurcations.

Once we have a common computational model for both bursting patterns, the transition from one pattern to the other is organized in parameter space by a codimension-2 bifurcation point, namely a *saddle-node homoclinic (SNH)* point (also referred to as *saddle-node separatrix loop bifurcation*, see [15]), in the vicinity of which one can generate bursting patterns of parabolic and square-wave types, respectively. At the boundary between these two bursting regimes, that is, in the vicinity of the SNH point in the plane of slow variables, one can obtain an intermediate bursting pattern, termed triangular or mixed-type, whose output looks like square-wave bursting for the initiation of the burst, and like parabolic bursting for the termination of the burst. The quiescent phase of mixed-type bursting trajectories has intermediate characteristics between the other two patterns; see the Results section and Fig. 4 for details.

2.4.1 Deterministic and stochastic versions of the model's equation:

The extended HR model used in the present work is composed by a set of four nonlinear differential equations, and it is deterministic. Its equations read:

$$\begin{aligned} \dot{x} &= c(x - x^3/3 - y + z + 2)\,, \\ \dot{y} &= (x^2 + d\,x - b\,y + a)/c\,, \\ \dot{z} &= -\varepsilon\,(-s\,(x - x_1) - b + b_0)\,, \\ \dot{b} &= \quad \varepsilon\,(z - z_0 + \alpha\,x)\,, \end{aligned} \tag{1}$$

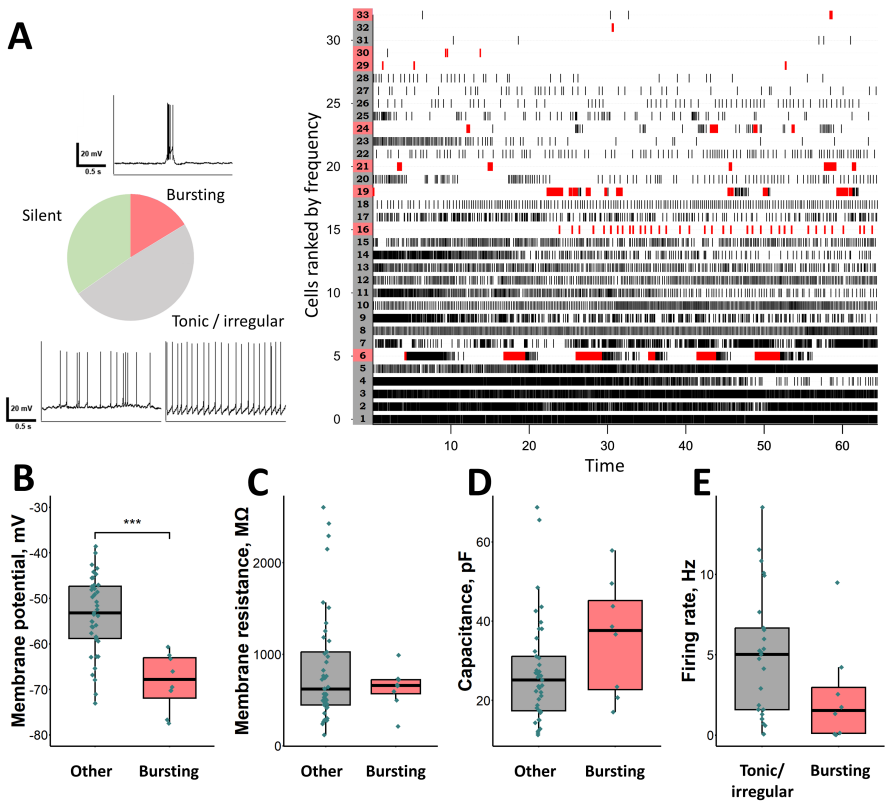

Figure 2: Spontaneous activity. (A) cell classification by spontaneous activity; 8 bursting cells, 25 tonic/irregular firing, and 17 silent. Above and below the pie chart: examples of cell activity. Left: raster plot of action potentials in cells ranked by mean spiking frequency. Bursting cells and individual bursts are highlighted in red. (B) Membrane potential, (C) membrane resistance and (D) membrane capacitance in bursting and other cells (including silent, $n = 41$). (E) Firing rate during the first 60 seconds of the recording, excluding silent cells (non-bursting $n = 25$).

the last two equations corresponding to a slow dynamics on (z, b) as a phenomenological way to include voltage-gated slow channel dynamics. The parameter values are fixed in all three bursting cases, except for parameters b_0, z_0 and α, which allow to switch between cases; see the caption of Fig. 1.

We also consider a stochastic version of system (1) by adding noise terms to the two slow equations, as an elementary way to mimic channel noise. The resulting stochastic differential equations (SDE) read:

$$\begin{aligned} \dot{X}_t &= c\,(X_t - X_t^3/3 - Y_t + Z_t + 2)\,, \\ \dot{Y}_t &= (X_t^2 + d\,X_t - b\,Y_t + a)/c\,, \\ \mathrm{d}Z_t &= -\varepsilon\,(-s\,(X_t - x_1 - b_t + b_0)\,\mathrm{d}t + \sigma_Z\,\mathrm{d}B_t^1\,, \\ \mathrm{d}b_t &= \quad \varepsilon\,(Z_t - z_0 + \alpha\,X_t)\,\mathrm{d}t + \sigma_C\,\mathrm{d}B_t^2\,. \end{aligned} \tag{2}$$

3 Results

3.1 Experimental results

To develop the model we began by characterizing neuronal dynamics of LHb neurons. We performed patch-clamp recordings in current-clamp configuration of 49 LHb neurons, of which 32 showed spontaneous spiking activity. Following previous publications, we classified its activity according to the spiking patterns into regular, non-regular, and bursting [28]. To identify and define bursts, we followed a statistical criterion based on the *Poisson Surprise method* (see methods). Using this criterion and in agreement with previous reports [3, 7, 22] only a small fraction of cells spontaneously displayed bursting activity (8 out of 32, Fig. 2 (a,b)).

Bursting cells were characterized by a more negative resting potential (-68.3 ± 6.34 mV for bursting neurons compared with -53.65 ± 8.41 mV for non-bursting neurons; $p = 0.0000965$ Student's t-test; $N = 41$ and 8 respectively, Fig. 2 C), and did not show differences in membrane resistance or capacitance (632.8 ± 220.9 MΩ vs. 842.0 ± 620.7 MΩ and 35.93 ± 14.5 pF vs. 27.1 ± 13 pF for bursting and non-bursting neurons, $p = 0.787$ and 0.103 respectively, Wilcox test, Fig. 2 D, E). In addition, the mean spiking frequency (excluding silent cells) was not significantly different between bursting and non-bursting neurons (2.44 ± 3.19 Hz vs. 5 ± 3.97 Hz for bursting and non-bursting cells, $p = 0.074$ Wilcox test, Fig. 2 F) supporting the notion that at the LHb bursting activity does not represent an increase in the average output.

To characterize the bursting activity of LHb neurons, we plotted individual bursts based on their duration and intra-burst frequency (Fig. 3(a)). In this space, the bursts are distributed following a continuous logarithmic distribution (Fig. 3 inset), where bursts with spiking frequencies higher than 75Hz are shorter than 200ms, and bursts longer than 1s exhibit mean intra-burst frequencies below 30Hz. The bursts in the short-duration and high-frequency tails of the distribution display typical square-wave burst features such as a low frequency towards the end of the burst and the fact that the burst occurs on a plateau of potential compared to the silent phase [24]. Conversely, the longer-duration and lower-frequency tail of the burst population includes events that could be categorized as parabolic bursts which, from the modeling viewpoint, are characterized by a lower frequency at the beginning and at the end of the burst and by the absence of a plateau during the burst [24]. Indeed, single mode bursting model of parabolic and square burst reproduce single bursts from LHb. In addition, this tail of the population includes mixed bursts that occur over a long-lasting depolarization plateau as a sequence of a square burst at the beginning that transitions into a parabolic burst at the end. These mixed bursts display high frequencies at the beginning that decrease and then remain constant or increase again (red bursts examples for cells 6 and 21). Notably, some LHb neurons exhibit both parabolic and square bursts (e.g., cells 6, 19, and 21 on Fig. 3). Notably, a single LHb neuron can display parabolic bursts, square bursts, tonic activity, and irregular activity (Fig. 3). Thus a mathematical model of LHb neurons should account for this wide range of behaviors.

Bursting activity is a prominent feature of LHb neurons and can be revealed upon hyperpolarization as rebound activity [22]. To gather data on the bursting properties from a larger fraction of LHb neurons, we evaluated their activity after hyperpolarizing pulses. Using this approach, the majority of LHb neurons (31/47) exhibited rebound bursting activity, which persisted as repeated bursts in 9 of these cells.

Next, we present simulations from both the deterministic and the stochastic versions of the model, and show that it accounts for the repertoire of dynamics behaviors observed at the LHb.

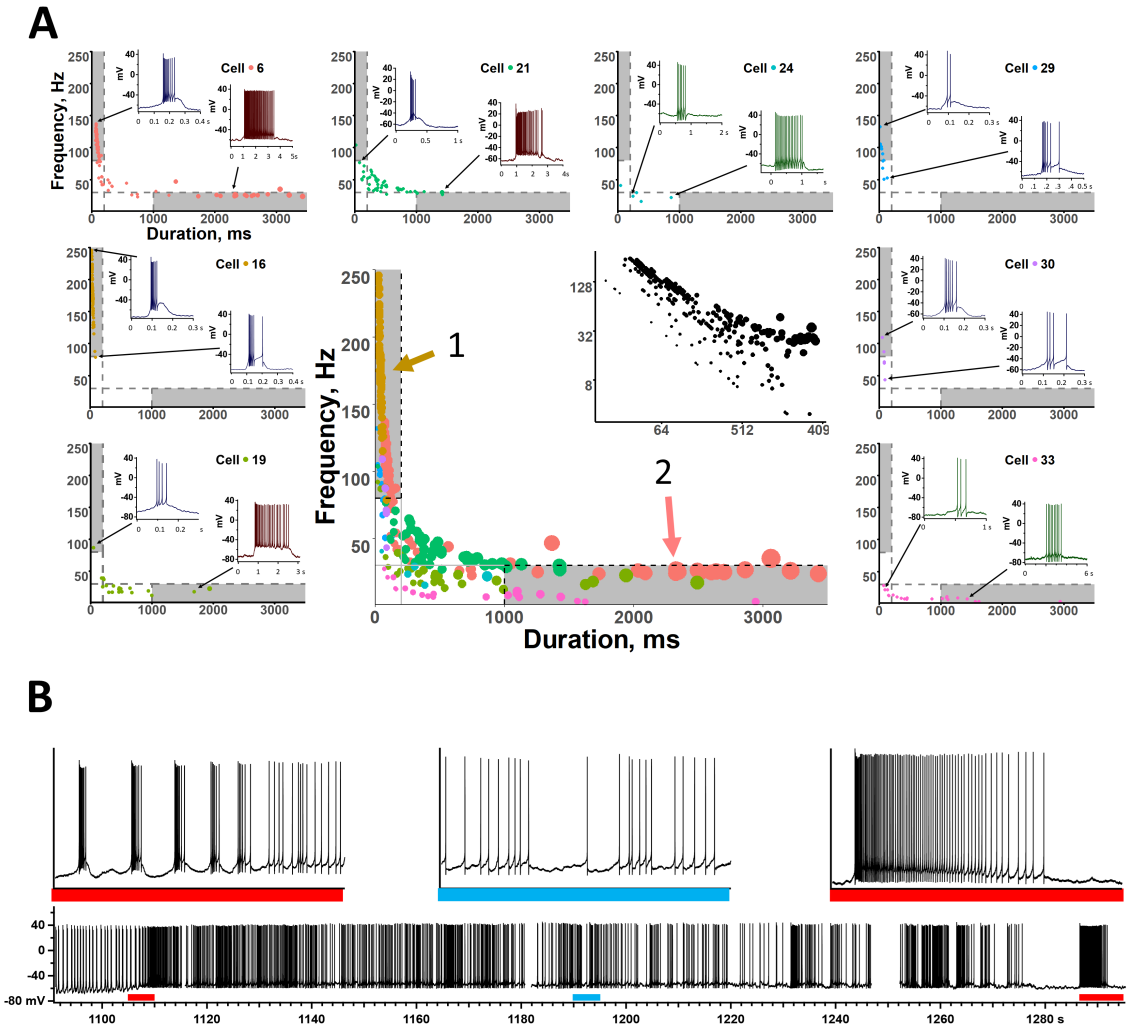

Figure 3: Spontaneous activity, burst features. (A) Plots of bursting duration vs. intra-burst spiking frequency for 8 spontaneously bursting cells. In the center: combined plot; inset (black): log scale. (B) Examples of behavior observed in cell 6; following a brief depolarization (not shown) cell develops and sustains periodic square bursts (left), which then transition to irregular tonic activity (center), and finally resolves into a stable behavior of long mixed or parabolic bursts. Individual cell numbers are consistent with Fig. 2.

3.2 Modelling results

System (1) has explicit timescale separation with two fast variables x and y, which mimic membrane potential and fast channel dynamics, respectively, and two slow variables z and b, which mimic slow channel dynamics. Standard slow-fast analysis consists in setting $\varepsilon = 0$ in system (1), which yields the so-called fast subsystem. In the fast subsystem, the slow variables become parameters and the main interest in studying the fast subsystem comes through its bifurcation structure with respect to these distinguished parameters. Indeed, when reinstating $\varepsilon = 0$, one realizes through numerical simulations (and can prove mathematically) that the full system's dynamics remain most of the time close to families of attractors (stationary or periodic) of the fast subsystem. When the system contains two slow variables, and hence the fast subsystem two distinguished parameters, the corresponding bifurcation diagram of interest is naturally a two-parameter bifurcation diagram, onto which it is useful and customary to superimpose solutions from the full system, projected onto this diagram; see Fig. 4. This approach is particularly suited to studying bursting dynamics in the full system, in which case the projection onto the plane of slow variables typically shows a slow path flowing across bifurcation curves of the fast subsystem. In particular, bifurcation of equilibria, e.g., saddle-node (SN) bifurcations and Hopf (HB) bifurcations, and bifurcation of limit cycles, e.g., saddle homoclinic (Hom) bifurcations and SNIC bifurcations. In Fig. 4, on top of the two-parameter bifurcation diagram system (1)'s fast subsystem with respect to z and b, are superimposed the three bursting trajectories shown in Fig. 1 (a2), (b2) and (c2), respectively,

projected onto the (z, b) plane. As explained above, this plotting strategy allows to shed important light onto the different bursting patterns depending on the region of parameter space visited by the slow dynamics. In the present case, the pattern corresponding to panel (a2) in Fig. 1 is of parabolic bursting type, the pattern corresponding to panel (b2) is of square-wave type, and the intermediate

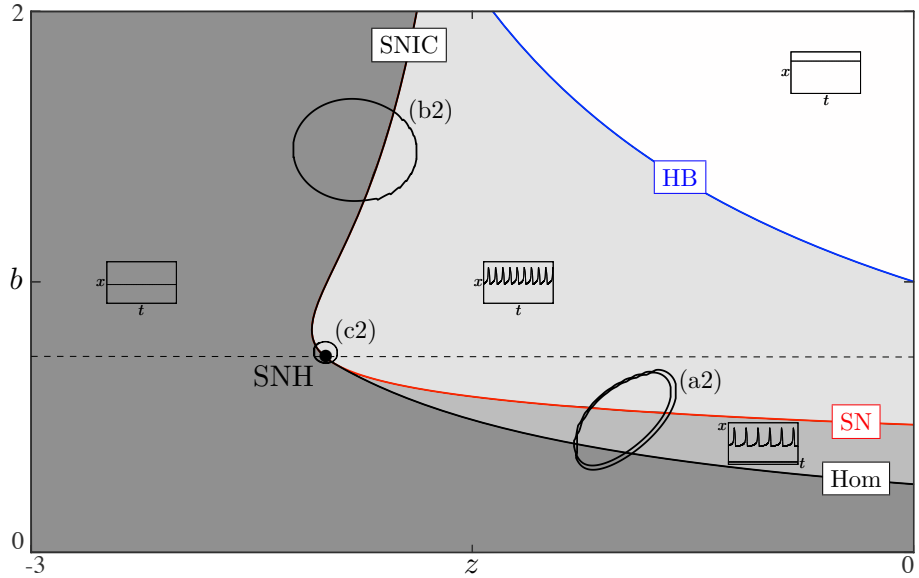

Figure 4: Two-parameter bifurcation diagram of the model's fast subsystems (i.e., when the slow variables' dynamics are frozen and replaced by parameters) explains the two main bursting patterns found, as well as, the intermediate one. The red curve correspond to a family of saddle-node bifurcations of equilibria labelled SN, the black curve corresponds to a family of homoclinic bifurcations, and the blue curve to a family of Hopf bifurcations. The first two curves meet at a codimension-2 bifurcation point called *saddle-node homoclinic* and labelled SNH. Above that point, in the two-parameter plane, the two curve coincide and correspond to a family of saddle-node on an invariant circle (labelled SNIC) bifurcation. Below SNH, the black curve corresponds to a family of saddle-homoclinic bifurcations labelled Hom. Round-shaped curves correspond to the slow evolution of parameters z and b. When the values of b stay below the SNH point, then the bursting pattern observed in the full system is of square-wave type and corresponds to the profile (a2) from Fig. 1. In contrast, if the value of b is located above the SNH point, then the observed bursting pattern in the full system is of parabolic type and it corresponds to the profile (b2) of Fig. 1. At the transition from one pattern to the other, we have trajectories of the full system that revolve around the SNH point, giving triangular (or mixed) bursting orbits like the one shown here, which corresponds to the profile (c2) of Fig. 1.

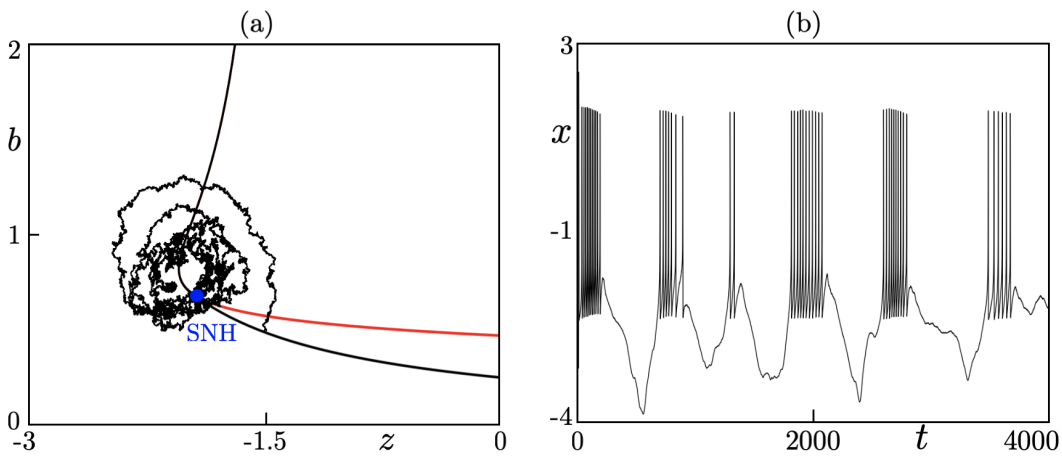

Figure 5: Simulation of the extended HR model with added stochastic input on the slow dynamics, system (2), leading to mixed bursting patterns. Fixed parameter values are as in Fig. 1, the other parameter values being: $b_0 = 0.8$, $z_0 = -1.8$, $\alpha = -0.1$, $\sigma_z = \sigma_b = 0.75$.

pattern corresponding to panel (c2) is of mixed type and indeed it revolves around the SNH point. All three patterns can be associated with the crossings of different bifurcation curves of the fast subsystem. Namely, parabolic bursting occurs when the slow variables drive the dynamics back and forth across a curve of SNIC bifurcations (black curve above the SNH point on Fig. 4), while square-wave bursting is the result of a slow passage through a curve of saddle-node bifurcations of equilibria (red curve) and a curve of saddle-homoclinic bifurcations (black curve below the SNH point). The mixed-type (triangular) bursting pattern corresponds to an initiation of the burst as the trajectory crosses the SN curve, and a termination of the burst as it crosses the SNIC curve, hence giving a mix of both main patterns. Square-wave and parabolic bursting patterns dominate and, loosely speaking, they correspond to cases where the slow variables evolve below and above, respectively, the SNH point; see the dashed line in Fig. 4. In contrast, the mixed-type bursting pattern is obtained from trajectories whose slow dynamics revolve around the SNH point.

The effect of noise on this two-parameter structure allows a switch from one pattern to the other one following a slow random path. This can produce time series where both bursting patterns are successively present Fig. 5 reproducing the behavior observed in LHb neurons.

4 Discussion

In the last decade, the LHb has been increasingly recognized as a central hub for the neural processing of aversive stimuli [13, 21, 23]. This conceptualization is supported by three key observations. First, the LHb exhibits systematic excitation in response to aversive stimuli. Second, its activation is intrinsically linked to negative motivational value.

From a physiological perspective, the LHb is characterized by low levels of intraconnectivity and a marked predominance of glutamatergic neurons. Consequently, its output is primarily shaped by the interplay of incoming synaptic inputs and the intrinsic properties of individual neurons. In vivo and in vitro, LHb neurons exhibit high basal activity and a diverse repertoire of spiking dynamics, which can be classified as silent, tonic, irregular, or bursting [29]. Surprisingly, no consistent link has been found between these spiking patterns and anatomical localization, cell morphology, or gene expression [11, 29]. Indeed, most LHb neurons can exhibit all four modes of activity depending on their membrane potential [7, 29]. Therefore, while future research may uncover physiological heterogeneity within LHb neurons, current evidence supports the practicality of describing LHb neurons with a single model as the one presented here.

In recent years, the bursting activity of the LHb has gained much attention since it has has been consistently associated with increases in negative motivational values [3, 4, 6, 7, 14, 19, 22, 26, 30]. In our experiments, the bursting activity in the LHb does not correspond to an increase in the mean spiking frequency of neurons, suggesting that the relationship between LHb bursting activity and increased negative motivational values may stem from the dynamics of the bursting itself, rather than from changes in the average neuronal output of the LHb neurons.

Bursting dynamics are a complex phenomenon that has been extensively studied in other neuronal populations, resulting in detailed modeling and classification [9, 15]. However, at the LHb, bursting activity has generally been characterized in broad terms, often as periods of high activity defined by absolute frequency criteria or left undefined altogether [4, 6, 7, 14, 19, 22, 26, 30], but see [3, 5]. Our work is a first step into systematic charactherization of bursting activity at the LHb.

Applying a simplified version of the well-accepted Poisson Surprise [18] and defining bursts in the space of intraburst frequency and duration, we identified a great diversity of bursting activity at the LHb. The population can be characterized by two extremes and intermediate behaviors. One extreme is defined by bursts shorter than 200ms, intraburst frequencies higher than 75Hz and prominent variance in the intraburst frequency domain. The absolute frequency criterion applied by other authors to identify bursts would include this tail of the population [7, 30, 4], which seems to correspond to square-wave bursts based on the fact that the burst occurs on a plateau compared to the quiescent phase, and that the frequency decreases along the burst. The second extreme includes long bursts ($> 1\,\mathrm{s}$) with lower spiking frequencies < 30Hz and prominent variance in the duration domain. This second tail of the population includes events that could be defined as parabolic bursts based on the absence of plateau during the burst and the frequency variation during the burst. However, in order to fully relate the statistical and the computational modeling approaches, we would need a refined strategy to identify bursts in time series that not only takes into account the time events (spike detection, time between two consecutive spikes as a proxy to identify a burst) but also the shape of the burst (on a plateau or not) as well as the evolution of the instantaneous spike frequency (monotonic or non-monotonic) along the burst. This is an

important aspect and an ongoing follow-up to the present work.

In the second tail, one can also observe the presence of mixed forms that begin as square-wave bursts and transition into parabolic bursts; from the modeling viewpoint, these are characterised as triangular (or mixed) bursting patterns and they occur at the transition between square-wave and parabolic bursting patterns, close to the codimension-2 SNH point [15]; see again Figs. 1 and 4.

These subpopulations of bursts might have been overlooked by previous works. However, it should be noted that *in vivo* the characteristic square depolarizing waves that define square-wave bursts would occur on top of a much higher basal spiking frequency, a consideration that leaves open the possibility that parabolic and mixed-type bursts were actually identified by the 20 ms inter-event interval used to define bursts by other authors [4, 7, 30]. Square-wave and parabolic bursts are different phenomena from both the pre- and postsynaptic perspectives. From the presynaptic point of view, these activity patterns are generated by different conductances. Square-wave bursts fit to the hyperpolarization induced bursts well described at the LHb by [30], which depends on low-threshold voltage dependent calcium channels and, to a less extent, on HCN channels. On the other hand, conductances underlying parabolic bursts are unknown at the LHb, and are less characterized in other neuronal systems, but could depend on persistent sodium channels and M type potassium channels [2, 10]. Therefore, both patterns of activity have different voltage dependence and could reflect different neuronal states.

From the postsynaptic perspective, square-wave and parabolic burst represent markedly different dynamics in the propagation of information to downstream structures. Short, high-frequency spiking events that define square bursts would propagate information dominated by feed-forward and short-term plasticity dynamics [16]. Conversely, long, low-frequency parabolic bursts would involve distinct short-term plasticity conditions and provide sufficient time for multi-synaptic negative and neuromodulatory feedback circuits to influence the propagation of information. Moreover, these two patterns of bursting behavior, along with tonic activity, could coexist in the same LHb neurons, revealing the potential of this structure to display state-dependent modes of information transmission [16, 17, 31]. The model we have developed includes all these behaviors and constitutes a first step to understand dynamic behaviors of LHb neurons. Future experimental and modeling work will shed light into the conductances underlying parabolic bursts and the physiological implications of the different bursting patterns on aversion encoding at the LHb.

Acknowledgments. SR is supported by the grant PID2023-146683OB-100 funded by MICIU/AEI /10.13039/501100011033 and by ERDF, EU. Additionally, he is supported by Ikerbasque Foundation and the Basque Government through the BERC 2022-2025 program and by the Ministry of Science and Innovation: BCAM Severo Ochoa accreditation CEX2021-001142-S / MICIU / AEI / 10.13039/501100011033. Moreover, SR acknowledges the financial support received from BCAM-IKUR, funded by the Basque Government by the IKUR Strategy and by the European Union NextGenerationEU/PRTR. DF, JP and SR also acknowledge support of SILICON BURMUIN no. KK-2023/00090 funded by the Basque Government through ELKARTEK Programme. JP acknowledges support by the Ikerbasque Basque Foundation for Science, EU COFUND H2020-MSCA-COFUND-2020-101034228-WOLFRAM2, and the Achucarro Basque Center for Neuroscience.

References

[1] M. E. Abraham, V. Ong, J. Gendreau, N. J. Brown, E. H. Choi, N. A. Shlobin, C. Y. Yang, S. Shahrestani, A. S. Himstead, D. K. Detchou, N. Patel, J. Gold, R. Sahyouni, L. D. Diaz-Aguilar, and S. Ben-Haim. Investigating deep brain stimulation of the habenula: A review of clinical studies. *Neuromodulation: Technology at the Neural Interface*, 26(2):292–301, 2023.

[2] R. J. Butera Jr, J. Rinzel, and J. C. Smith. Models of respiratory rhythm generation in the pre-botzinger complex. i. bursting pacemaker neurons. *Journal of Neurophysiology*, 82(1):382–397, 1999.

[3] I. Cerniauskas, J. Winterer, J. W. de Jong, D. Lukacsovich, H. Yang, F. Khan, J. R. Peck, S. K. Obayashi, V. Lilascharoen, B. K. Lim, et al. Chronic stress induces activity, synaptic, and transcriptional remodeling of the lateral habenula associated with deficits in motivated behaviors. *Neuron*, 104(5):899–915, 2019.

[4] M. Chen, S. Ma, H. Liu, Y. Dong, J. Tang, Z. Ni, Y. Tan, C. Duan, H. Li, H. Huang, Y. Li, X. Cao, C. J. Lingle, Y. Yang, and H. Hu. Brain region–specific action of ketamine as a rapid antidepressant. *Science*, 385(6709):eado7010, 2024.

[5] D. Cobb-Lewis, A. George, S. Hu, K. Packard, M. Song, I. Nikitah, O. Nguyen-Lopez, E. Tesone, J. Rowden, J. Wang, and M. Opendak. The lateral habenula integrates age and experience to promote social transitions in developing rats. *Cell Reports*, 43(8):114556, 2024.

[6] Y. Cui, S. Hu, and H. Hu. Lateral habenular burst firing as a target of the rapid antidepressant effects of ketamine. *Trends in Neurosciences*, 42(3):179–191, 2019.

[7] Y. Cui, Y. Yang, Z. Ni, Y. Dong, G. Cai, A. Foncelle, S. Ma, K. Sang, S. Tang, Y. Li, et al. Astroglial kir4. 1 in the lateral habenula drives neuronal bursts in depression. *Nature*, 554(7692):323–327, 2018.

[8] M. Desroches, M. Krupa, and S. Rodrigues. Spike-adding in parabolic bursters: the role of folded-saddle canards. *Physica D: Nonlinear Phenomena*, 331:58–70, 2016.

[9] M. Desroches, J. Rinzel, and S. Rodrigues. Classification of bursting patterns: A tale of two ducks. *PLoS Computational Biology*, **18**(2):e1009752, 2022.

[10] D. Golomb, C. Yue, and Y. Yaari. Contribution of persistent na+ current and m-type k+ current to somatic bursting in ca1 pyramidal cells: combined experimental and modeling study. *Journal of Neurophysiology*, 96(4):1912–1926, 2006.

[11] Y. Hashikawa, K. Hashikawa, M. A. Rossi, M. L. Basiri, Y. Liu, N. L. Johnston, O. R. Ahmad, and G. D. Stuber. Transcriptional and spatial resolution of cell types in the mammalian habenula. *Neuron*, 106(5):743–758, 2020.

[12] J. L. Hindmarsh and R. M. Rose. A model of neuronal bursting using three coupled first order differential equations. *Proceedings of the Royal Society of London B: Biological Sciences*, **221**(1222):87–102, 1984.

[13] H. Hu, Y. Cui, and Y. Yang. Circuits and functions of the lateral habenula in health and in disease. *Nature Reviews Neuroscience*, 21(5):277–295, 2020.

[14] L. Huang, Y. Xi, Y. Peng, Y. Yang, X. Huang, Y. Fu, Q. Tao, J. Xiao, T. Yuan, K. An, et al. A visual circuit related to habenula underlies the antidepressive effects of light therapy. *Neuron*, 102(1):128–142, 2019.

[15] E. M. Izhikevich. Neural excitability, spiking and bursting. *International Journal of Bifurcation and Chaos*, 10(06):1171–1266, 2000.

[16] E. M. Izhikevich, N. S. Desai, E. C. Walcott, and F. C. Hoppensteadt. Bursts as a unit of neural information: selective communication via resonance. *Trends in Neurosciences*, 26(3):161–167, 2003.

[17] A. Kepecs and J. Lisman. How to read a burst duration code. *Neurocomputing*, 58:1–6, 2004.

[18] C. R. Legendy and M. Salcman. Bursts and recurrences of bursts in the spike trains of spontaneously active striate cortex neurons. *Journal of Neurophysiology*, 53(4):926–939, 1985. PMID: 3998798.

[19] K. Ma, H. Gu, and Y. Jia. The neuronal and synaptic dynamics underlying post-inhibitory rebound burst related to major depressive disorder in the lateral habenula neuron model. *Cognitive Neurodynamics*, 18(3):1397–1416, 2024.

[20] S. Ma, M. Chen, Y. Jiang, X. Xiang, S. Wang, Z. Wu, S. Li, Y. Cui, J. Wang, Y. Zhu, et al. Sustained antidepressant effect of ketamine through nmdar trapping in the lhb. *Nature*, 622(7984):802–809, 2023.

[21] L. Michel, P. Molina, and M. Mameli. The behavioral relevance of a modular organization in the lateral habenula. *Neuron*, 2024.

[22] S. Mondoloni, P. Molina, S. Lecca, C.-H. Wu, L. Michel, D. Osypenko, F. Cachin, M. Flanigan, M. Congiu, A. L. Lalive, T. Kash, F. Deng, Y. Li, and M. Mameli. Serotonin release in the habenula during emotional contagion promotes resilience. *Science*, 385(6713):1081–1086, 2024.

[23] C. D. Proulx, O. Hikosaka, and R. Malinow. Reward processing by the lateral habenula in normal and depressive behaviors. *Nature Neuroscience*, 17(9):1146–1152, 2014.

[24] J. Rinzel. A formal classification of bursting mechanisms in excitable systems. In *International Congress of Mathematicians, Berkeley, California, USA, August 3-11, 1986*, volume **II**, pages 1578–1593. American Mathematical Society, 1987.

[25] J. S. Rothman and R. A. Silver. Neuromatic: An integrated open-source software toolkit for acquisition, analysis and simulation of electrophysiological data. *Frontiers in Neuroinformatics*, 12, 2018.

[26] J.-S. Seo, P. Zhong, A. Liu, Z. Yan, and P. Greengard. Elevation of p11 in lateral habenula mediates depression-like behavior. *Molecular Psychiatry*, 23(5):1113–1119, 2018.

[27] J. T. Ting, B. R. Lee, P. Chong, G. Soler-Llavina, C. Cobbs, C. Koch, and Lein E. Zeng, H. Preparation of acute brain slices using an optimized n-methyl-d-glucamine protective recovery method. *JoVE*, (132):e53825, 2018.

[28] F. Wagner, T. Weiss, and R. W. Veh. Electrophysiological properties of neurons and synapses in the lateral habenular complex (lhb). *Pharmacology Biochemistry and Behavior*, 162:38–45, 2017.

[29] T. Weiss and R. W. Veh. Morphological and electrophysiological characteristics of neurons within identified subnuclei of the lateral habenula in rat brain slices. *Neuroscience*, 172:74–93, 2011.

[30] Y. Yang, Y. Cui, K. Sang, Y. Dong, Z. Ni, S. Ma, and H. Hu. Ketamine blocks bursting in the lateral habenula to rapidly relieve depression. *Nature*, 554(7692):317–322, 2018.

[31] F. Zeldenrust, W. J. Wadman, and B. Englitz. Neural coding with bursts—current state and future perspectives. *Frontiers in Computational Neuroscience*, 12:48, 2018.